Biosensors and Bioelectronics xxx (2008) xxx–xxx

Contents lists available at ScienceDirect

Biosensors and Bioelectronics

journal homepage: www.elsevier.com/locate/bios

# Design rule for optimization of microelectrodes used in electric cell-substrate impedance sensing (ECIS)

Dorielle T. Price, Abdur Rub Abdur Rahman, Shekhar Bhansali*

*BioMEMS and Microsystems Laboratory, Dept. of Electrical Engineering, University of South Florida, 4202 East Fowler Avenue, ENB 118, Tampa, FL 33620, United States*

ARTICLE INFO

*Article history:*
Received 26 August 2008
Received in revised form 21 October 2008
Accepted 24 October 2008
Available online xxx

*Keywords:*
ECIS optimization
Passivation coating capacitance
Microelectrode

ABSTRACT

This paper presents an experimentally derived design rule for optimization of microelectrodes used in electric cell-substrate impedance sensing (ECIS) up to 10 MHz. The effect of change in electrode design (through electrode sensor area, lead trace widths, and passivation coating thickness) on electrode characteristics was experimentally evaluated using electrochemical impedance spectroscopy (EIS) measurements and analyzed using equivalent circuit models. A parasitic passivation coating impedance was successfully minimized by designing electrodes with either a thicker passivation layer or a smaller lead trace area. It was observed that the passivated lead trace area to passivation coating thickness ratio has a critical value of 5.5, under which the impedance contribution of the coating is minimized. The optimized design of ECIS-based microelectrode devices reported in this work will make it possible to probe the entire beta dispersion region of adherent biological cell layers by reducing measurement artifacts and improving the quality of data across the beta-dispersion region. The new design will enable the use of the commonly used ECIS technique to measure real-time cellular properties in high frequency ranges (beta dispersion) that was not possible thus far.



## 1. Introduction

Microelectrode-based impedance characterization of biological cells is emerging as a diagnostic tool for studying electrophysiological and biophysical changes due to viral infections (McCoy and Wang, 2005), cancer detection (Aberg et al., 2004), and drug response (Huang et al., 2003). Advantages of using microelectrodes over conventional electrodes include: economy due to batch fabrication (Judy, 2001), large current densities (with low currents) due to enhanced mass transport (Justin et al., 2008) and the ability to integrate electrodes with other instrumentation to develop portable measurement systems (Park and Shuler, 2003). Microelectrodes, due to smaller currents, have the potential to perform non-destructive measurements and facilitate the study of high resistivity samples (Matysik et al., 1995). A disadvantage of microelectrodes is that they have much higher impedances compared to macroelectrodes due to the interfacial capacitance. Interfacial, or double layer, capacitance arises from the interactions between ions and molecules at the interface of the electrolyte and electrode surface and has been established to be indirectly proportional to the electrode area (Franks et al., 2005). This double layer capacitance places a constraint on the measurement equipment and increases the measurement error. Consequently, microelectrode designs need to be optimized to reduce interfacial impedance as well as to extend the useful high frequency probing range of the microelectrode, without being limited by device parasitics. In bioimpedance spectroscopy measurements of cell cultures, one such high frequency parasitic is caused by the passivated metallic areas (lead traces or tracks), which serve to connect the sensing electrode to the contact pads that interface with the measurement electronics. This parasitic impedance, referred to in this manuscript as coating impedance, is superimposed on the measured impedance of the electrode–electrolyte system, thus distorting the measured data and complicating its analysis (Rahman et al., 2007). The reduction of the parasitic components is critical for electrophysiological studies in cell-based systems.

Electroanalytical approaches to cellular studies are being increasingly investigated due their ability to detect cellular and subcellular interactions (Adams et al., 2008). Electrode design optimization of microelectrodes is critical to the efficient employment of these techniques in drug discovery, clinical diagnostics and electrophysiology. A geometrically optimized sensor for bioimpedance measurements can result in an increased measurement range and decreased noise. Pejcic and De Marco (2006) reiterate that sensor optimization is one of the most crucial steps in the realization of an electroanalytical device.

* Corresponding author. Tel.: +1 813 974 3593; fax: +1 813 974 5250.
*E-mail address:* bhansali@eng.usf.edu (S. Bhansali).
*URL:* http://www.mems.eng.usf.edu/ (S. Bhansali).

0956-5663/$ – see front matter © 2008 Elsevier B.V. All rights reserved.
doi:10.1016/j.bios.2008.10.026

Researchers have performed experiments to optimize the electrode designs for various applications. Fosdick and Anderson (1986) optimized the geometry of a microelectrode array flow detector; with respect to amperometric response; and Min et al. (2004) investigated geometric parameters (i.e. electrode height, material, gap size, and electrode width) of interdigitated ultramicroelectrode arrays (IDUAs) to optimize oxidation and reduction reactions of ferro/ferrihexacyanide. Sandison et al. (2002) studied electrode sensor array geometry (center-to-center spacing and diameter) and porosity of electrode sensors using $Si_3N_4$-coated silicon substrate and Lempka et al. (2006) optimized silicon-substrate microelectrodes for neural activity recordings. All of these optimizations were application specific.

While the aforementioned works studied the optimization of electrodes for flow detectors, neural recordings, and microfluidic biosensors; design rules for optimization of microelectrodes for ECIS-based measurements had received little attention in published literature and is being increasingly looked at. Wang et al. (2008) investigated the sensitivity and frequency characteristics of interdigitated array microsensors for ECIS. Rahman et al. (2007) recently demonstrated the effect of high frequency parasitic coating impedance on ECIS measurements and successfully developed a comprehensive model which confirmed the impedance contribution of passivated lead trance capacitance, lead trace resistance and inductance at higher frequencies. This work systematically minimized the effect of parasitics by varying parameters such as electrode area and lead trace width. Equivalent circuit modeling of the complex impedance data confirms that the coating parasitics at high frequencies are indeed minimized by the optimization criteria developed in this work. This enables useful bipolar impedance data analysis up to 10 MHz, the maximum frequency of the beta dispersion range of biological cells.

Schwan (1963) identified three major biological dispersion regions, namely, alpha ($\alpha$), beta ($\beta$), and gamma ($\gamma$), at low, mid, and high frequencies respectively. The region of interest in this paper is the beta dispersion, usually between $10^4$ and $10^7$ Hz, which provides information about the cell membrane—of significant relevance in the study of electroporation mediated drug delivery.

In literature, research groups have used various microelectrode designs specific for differing biomedical applications. In example, Gomez et al. used SiC probes to perform impedance measurements in living tissues. It was shown that the SiC substrate reduced the current leakage, compared to a Si substrate; however, a parasitic capacitance component remained above 10 kHz (Gómez et al., 2006). The high-frequency parasitic was attributed to the capacitive coupling of wires and contact pad interfaces; however, this assumption was not clearly established. The capacitive parasitic could be attributed to the thin $SiO_2/Si_3N_4$ (300 nm/700 nm) passivation layer. Franks et al. designed microelectrodes passivated with 500 nm of $Si_3N_4$ for use in biomedical applications. Above 10 kHz, the impedance phase of the measured electrolyte began to turn negative from 0°, suggesting a parasitic capacitance component. This parasitic component was not acknowledged, and the measured data was modeled as an R-CPE (constant phase element) series circuit (Franks et al., 2005). Because the high-frequency capacitive component was not accounted for, the modeled results, did not overlap the measured data above 10 kHz; thus affecting the accuracy of the extracted system parameters. Other examples of the effect of the high-frequency parasitic capacitance on measurement range can be found in (Ivorra et al., 2003; Yun et al., 2007). The microelectrodes used in the aforementioned experiments have the potential to be optimized by increasing the thickness or decreasing the area of the passivation layer according to the derived design rule; hence suppressing the parasitic capacitance and extending the measurement range up to 10 MHz.

This paper addresses the optimization of the parasitic coating impedance to facilitate the characterization of anchorage dependent cells. The design criteria developed in this research led to the elimination of the passivation coating component.

## 2. Materials and methods

### 2.1. Fabrication of microelectrodes

Gold microelectrode devices were fabricated on 4-in. glass wafers using photolithography and metal deposition techniques. The fabrication process flow is illustrated in Fig. 1(a–f). First the wafers were cleaned and thin layers of chromium (Cr) and gold (Au) were thermally evaporated onto the glass. Next, the electrode traces, sensors, and contact pads were lithographically defined using S1813 photoresist. The patterned wafer was then electroplated. The wafer was solvent cleaned to remove the photoresist, and then the evaporated Au and Cr were selectively removed via wet etching to define the metal patterns on the substrate. Finally, a second lithography step was performed to apply the passivation coating (photoresist) layer. In this step, only the electrode sensors and contact pads were exposed to make contact with the electrolyte; the rest of the metal area constituting the lead trace connecting the electrode to the measurement contact pads are buried under the polymer resin layer. The photoresist was hard baked to impart stability and inertness to the polymer. S1813 resist was used as the 2 μm-thick coating and AZ 4620 resist was used as the 20 μm-thick coating. The wafers were diced into single devices and cloning cylinders were attached to serve as the electrolyte reservoir. The cylinders were centered and attached around the four sensors by slowly heated photoresist around the outer circumference of cylinder, using a hotplate. Subsequently, the photoresist harden as it slowly cooled and to form a tight seal with few air pockets. The 500 and 30 μm trace-width devices are illustrated in Fig. 1g and h, respectively.

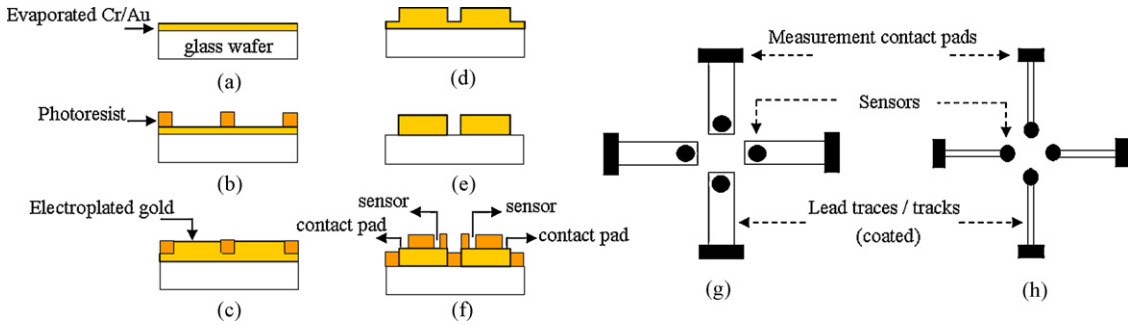


**Fig. 1.** (a–f) Fabrication process for microelectrode devices; top-view schematics of 500 μm trace-width device (g); 30 μm trace-width device (h).

Please cite this article in press as: Price, D.T., et al., Biosens. Bioelectron. (2008), doi:10.1016/j.bios.2008.10.026

Electrode devices with different sensors diameters were fabricated for each trace width. The 500 μm trace-width devices had sensor diameters of 500, 250, and 100 μm. Similarly, the 30 μm trace-width devices had sensor diameters of 500, 250, and 125 μm.

### 2.2. Experimental setup

A Cascade microprobe station (Cascade Microtech, Beaverton, OR) was used to make contact with the contact pads of the electrodes, thus connecting the devices to the impedance analyzer. The probe tips were cleaned with Probe Polish, PN 134-209 (Cascade Microtech), to remove any oxide buildup that could potentially cause unstable measurements. An Agilent 4294A Impedance Analyzer was used in this experiment to measure impedance. The measurement conditions were: 10 mV peak-to-peak excitation applied over a frequency range of 100 Hz to 10 MHz at room temperature, with no applied DC bias. Before measurements were made, the system was calibrated using capacitive and resistive calibration standards and compensated for measurement cable effects using the standard protocol supplied by the manufacturer (Agilent, 2003).

## 3. Theory

The capacitance of a polymer coating can be represented by the by the following expression:

$$C = \frac{\varepsilon_o \varepsilon_r A}{d} \quad (1)$$

where $\varepsilon_o = 8.86 \times 10^{-14}$ F/cm (permittivity of free space), $\varepsilon_r$ is the relative permittivity of the coating, $A$ is the area of the coating exposed to the electrolyte, and $d$ is the thickness of the coating. According to this equation, when the coating thickness is increased, the capacitance, which is inversely related to impedance, decreases. When the impedance of the coating is greater than the impedance of the spreading resistance (Table 1), more current will flow through the solution versus the coating; thereby minimizing the effect of coating capacitance component on the overall impedance of the electrochemical system.

For two similar electrodes in series, the spreading resistance can be approximated using the following equation, according to (Sagues and Kranc, 1996):

$$R_{sp} = \frac{2\rho}{4r} \quad (2)$$

**Table 1**
Theoretical parameters (coating area, coating capacitance, coating impedance, and spreading resistance) for all electrode configurations. The blanks (–) indicate that there is no sensor diameter corresponding to the specified trace-width device.

| | | 500 μm trace-width device | | 30 μm trace-width device |
|---|---|---|---|---|
| | | 2 μm-thick resist | 20 μm-thick resist | 2 μm-thick resist |
| 500 μm sensor | Coating area ($mm^2$) | 0.807 | 0.807 | 6.90E-02 |
| | Coating capacitance (F) | 1.79E-11 | 1.79E-12 | 1.53E-12 |
| | Coating impedance (at 10 MHz) (Ω) | 8.90E+02 | 8.90E+03 | 1.04E+04 |
| | Spreading resistance (Ω) | 1.40E+03 | 1.40E+03 | 1.40E+03 |
| 250 μm sensor | Coating area ($mm^2$) | 1.10 | 1.10 | 7.65E-02 |
| | Coating capacitance (F) | 2.44E-11 | 2.44E-12 | 1.69E-12 |
| | Coating impedance (at 10 MHz) (Ω) | 6.53E+02 | 6.53E+03 | 9.39E+03 |
| | Spreading resistance (Ω) | 2.80E+03 | 2.80E+03 | 2.80E+03 |
| 125 μm sensor | Coating area ($mm^2$) | – | – | 8.03E-02 |
| | Coating capacitance (F) | – | – | 1.78E-12 |
| | Coating impedance (at 10 MHz) (Ω) | – | – | 8.95E+03 |
| | Spreading resistance (Ω) | – | – | 5.60E+03 |
| 100 μm sensor | Coating area ($mm^2$) | 1.18 | 1.18 | – |
| | Coating capacitance (F) | 2.62E-11 | 2.62E-12 | – |
| | Coating impedance (at 10 MHz) (Ω) | 6.07E+02 | 6.07E+03 | – |
| | Spreading resistance (Ω) | 7.00E+03 | 7.00E+03 | – |

Please cite this article in press as: Price, D.T., et al., Biosens. Bioelectron. (2008), doi:10.1016/j.bios.2008.10.026

where $\rho$ is the resistivity of the solution in ohm-cm, and r is the radius of the electrode sensors. Spreading resistance (or constriction resistance) is defined by the well created by the passivation coating surrounding the sensors (see Fig. 1f). Theoretical spreading resistance values for the sensor geometries used in this study are listed in Table 1.

From Table 1 it is observed that the capacitance decreases as the area of the coating decreases. Therefore, decreasing the polymer-covered trace area should decrease the coating capacitance. In previous work by Rahman et al., experiments were performed on electrode devices with a 500 μm trace width and 2 μm-thick resist. The area of coating exposed to the electrolyte was approximately 1 $mm^2$, and the coating impedance appeared at approximately 1 MHz (Rahman et al., 2007). This is a result of more current flowing through the coating, a pathway of lower resistance. To validate this model, new electrode devices were designed and fabricated with a 30 μm trace-width; thus reducing the coating area to approximately $7.65 \times 10^{-2}$ $mm^2$, more than an order of magnitude smaller than the devices with a 500 μm trace width.

## 4. Results and discussion

### *4.1. Effect of increasing the passivation coating thickness on 500 μm trace-width devices of various electrode diameters (500, 250, and 125 μm)*

Impedance measurements were performed on the 500 μm trace-width devices to investigate the effect of increasing the coating thickness on the high-frequency impedance measurements using a simple binary electrolyte, potassium chloride (KCl). When the resist thickness was increased from 2 to 20 μm, there was a significant reduction in the coating impedance component, especially on the larger-diameter devices. A comparison of measurements with 2 μm- and 20 μm-thick coatings is illustrated in the bode plot of Fig. 2a.

From Table 1, the coating impedance calculated at 10 MHz is less than the spreading resistance for the devices with 2 μm-thick coating for all sensor diameters; hence current will flow through the coating as seen with the 250 μm sensor diameter, 2 μm-thick resist ('□') trace in Fig. 2a. In contrast, the coating impedance of the devices with 20 μm-thick coating is less than the spreading resistance for sensor diameters less than 250 μm (Table 1); so the coating capacitance component is not seen on the 250 μm ('◊') and 500 μm ('*') traces in Fig. 2a, however it is slightly apparent in the 100 μm sensor diameter, 20 μm thick resist ('×') trace.

As the coating impedance is less than the spreading resistance, the current tends to flow through the coating rather than the solution, causing the high-frequency coating component. The results confirm that increasing the coating thickness to 20 μm eliminates the coating component for devices with sensor diameters of 250 μm or greater.

### *4.2. Effect of decreasing the coating area (new devices: 30 μm trace width)*

To study the effect of trace width, electrodes were designed and fabricated with 30 μm trace width and impedance was measured using KCl as the electrolyte. Decreasing the coating area from 1.1 to $7.65 \times 10^{-2}$ $mm^2$ eliminated the high-frequency coating component on all measured sensors, including the 500, 250, 125 μm-diameter sensors, as illustrated in Fig. 2b.

Table 1 compares the theoretical coating capacitances and impedances of the two different coating areas, to theoretically illustrate the effect of reduced trace area on coating impedance. The theoretical coating impedances (at 10 MHz) of the

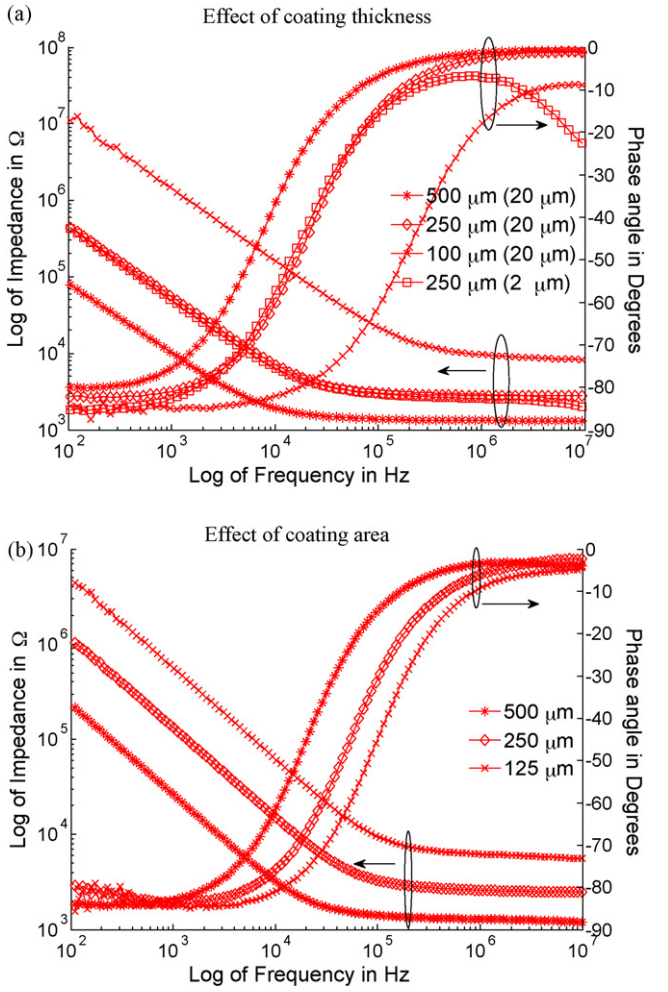


**Fig. 2.** (a) Bode plot of 500 μm trace-width devices, of varying sensor diameters, with 2 μm-thick resist and 20 μm-thick resist. (*) 500 μm sensor diameter, 20 μm thick resist; (◊) 250 μm sensor diameter, 2 μm thick resist; (×) 100 μm sensor diameter, 20 μm thick resist; (□) 250 μm sensor diameter, 20 μm thick resist. Increasing the coating thickness to 20 μm suppressed the coating impedance contribution. (b) Bode plot of 30 μm trace-width devices with 2 μm-thick coating of varying sensor diameters. (*) 500 μm sensor; (◊) 250 μm sensor, (×) 125 μm sensor. Decreasing the coating area suppressed the coating impedance contribution.

30 μm trace-width devices average $9.6 \times 10^3$ Ω, a value greater than the spreading resistances of the 500 μm diameter sensor ($R_{sp} = 1.4 \times 10^3$ Ω), 250 μm diameter sensor ($R_{sp} = 2.8 \times 10^3$ Ω) and 125 μm-diameter sensor ($R_{sp} = 5.6 \times 10^3$ Ω). This demonstrates that theoretically as well as experimentally, the coating component is no longer dominant at high frequencies with the reduced coated area of the 30 μm trace-width devices.

By removing the high-frequency coating component, the equivalent circuit of the KCl–electrode system was simplified from that shown in Fig. 3a to a resistor-constant phase element (CPE) series circuit shown in Fig. 3b. The bode plot in Fig. 3c shows a fit of the measured data from the 250 μm diameter sensor on the 30 μm trace-width device. The simplified R-CPE series circuit was used to fit the data and the extracted parameters are shown in 3d.

### *4.3. Experimentally derived design ratio: coating area to coating thickness*

The coating area is defined as the area of the polymer-covered lead trace in contact with the electrolyte (within the cylinder). The coating area was calculated with the following assumptions: (1)

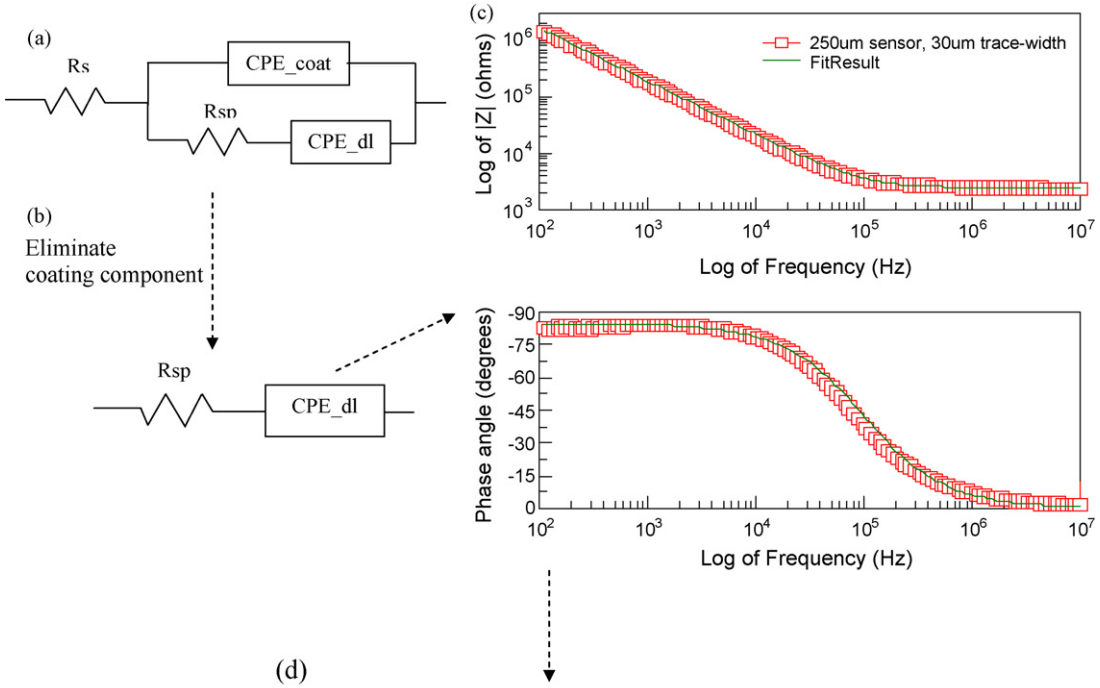


(d)

| | Fit Value | % error |
|---|---|---|
| CPE_dl (F-s(n-1)) | 1.36E-09 | 2.07 |
| n_dl | 0.944 | 3.32 |
| Rsp (Ω) | 2482 | 0.212 |
| chi-squared | | 2.53 |

**Fig. 3.** Equivalent circuit of KCl–electrode system: (a) with coating capacitance component and (b) without coating component; (c) measured data (250 μm sensor, 2 μm-thick resist, 30 μm trace-width device) fit with simplified R-CPE equivalent circuit; (d) extracted parameters from fit.

the arc formed by the cylinder across the traces was assumed linear and (2) the majority of the current flowed between the two traces. Fig. 4 is a schematic of the 500 and 30 μm trace-width devices with labeled parameters used in calculating the coating area.

Based on the aforementioned assumptions, a formula was derived for calculating the coating area on the 500 μm trace-width device, shown in Eq. (3):

$$\text{coating area}_{500\,\mu\text{m track}} = \left(D - S - 2 \times \pi\left(\frac{d}{2}\right)^2\right) \times W \quad (3)$$

where $D$ = 3.4 mm (inner diameter of cylinder), $S$ = 10 mm (center to center distance between electrodes), $d$ = diameter of electrode sensors, $W$ = 500 μm (width of electrode traces).

The top half of Table 2 shows the calculated ratios of coating area to coating thickness for the 500 μm trace-width devices. The highlighted ratios are for those electrode configurations in which a coating capacitance component was not present in impedance measurements up to 10 MHz.

From the data in Table 2, the following inequality is derived:

$$\frac{\text{coating area}}{\text{coating thickness}} < 5.5 \quad (4)$$

If the ratio of coating area to coating thickness is less than 5.5, then a coating capacitance will not be present in impedance measurements up to 10 MHz. This design rule was verified by designing electrodes according to this criteria and analyzing the resulting impedance data.

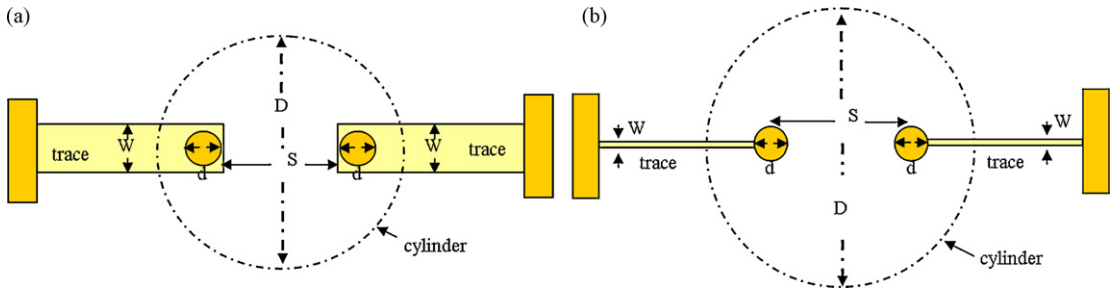


**Fig. 4.** Schematic of (a) 500 μm trace-width device and (b) 30 μm trace-width device showing the parameters used to calculate the coating area.

Please cite this article in press as: Price, D.T., et al., Biosens. Bioelectron. (2008), doi:10.1016/j.bios.2008.10.026

**Table 2**
Ratio of coating area to coating thickness for 500 μm trace-width devices of with varying sensor diameters. A coating capacitance component was not present in designs with an enclosed ratio.

| | Coating area ($mm^2$) | Ratio coating area / thickness (2 μm thick coating) | Ratio coating area / thickness (20 μm thick coating) |
|---|---|---|---|
| **500 μm trace-width device** | | | |
| 500μm sensor | 0.807 | 40.37 | **4.04** |
| 250μm sensor | 1.10 | 55.09 | **5.51** |
| 100μm sensor | 1.18 | 59.21 | 5.92 |
| **30 μm trace-width device** | | | |
| 500μm sensor | 6.90E-02 | **3.45** | |
| 250μm sensor | 7.65E-02 | **3.83** | |
| 125μm sensor | 8.03E-02 | **4.01** | |

The coating area for the 30 μm trace-width device is shown in Eq. (5):

$$\text{coating area}_{30\,\mu\text{m track}} = (D - S - d) \times W \quad (5)$$

where $D$ = 4.4 mm (inner diameter of cylinder), $S$ = 1.6 mm (spacing between electrode traces), $d$ = diameter of electrode sensors, $W$ = 30 μm (width of electrode traces).

A coating capacitance component was not seen in the 500, 250, and 125 μm-diameter sensors of the 30 μm trace-width devices (Fig. 2b). The bottom half of Table 2 shows that the coating area to coating thickness ratio for all sensor diameters fell below the critical value of 5.5, previously derived (Eq. (4)); thus verifying the design rule.

### 4.4. Design rule applied to ECIS commercial device

The 8W1E ECIS cell culture impedance device has a coated area of approximately 14 $mm^2$. For a coating thickness of 2 μm, the coating area to coating thickness ratio is calculated to be approximately 700, which is much greater than the critical ratio of 5.5. From this calculation, it can be inferred that the 8W1E ECIS device has a coating capacitance component at high frequencies. This was verified with previous measurements (Justin et al., 2008; Rahman et al., in press).

## 5. Conclusion

It has been experimentally proven that microelectrode devices, particularly those used for ECIS measurements, can be optimized by decreasing the coating (trace) area and/or increasing the coating thickness to eliminate the high-frequency coating component. A relationship between coating area and coating thickness was derived to aid in the design of ECIS-based microelectrode devices for high-frequency impedance measurements. A critical ratio of 5.5 (coating area to coating thickness) was defined in order to completely eliminate the coating capacitance component. Previously measurement data was truncated due to this noise; however, with the coating component removed, more information about the system under test is revealed and measurements can be made up to higher frequencies, in this case 10 MHz.

The redesigned system reduces measurement artifacts and improves the quality of data across the beta-dispersion region. The new design will enable the use of the commonly used ECIS technique to measure real-time cellular properties in high frequency ranges (beta dispersion) that was not possible thus far.

## Acknowledgements

This research was supported by NSF CAREER Award 0239262. This material is based upon work supported under a National Science Foundation Graduate Research Fellowship (NSF GRF), providing support to Dorielle Price.

## References

Aberg, P., Nicander, I., Hansson, J., Geladi, P., Holmgren, U., Ollmar, S., 2004. IEEE Trans. Biomed. Eng. 51, 2097–2102.
Adams, K.L., Puchades, M., Ewing, A.G., 2008. Annu. Rev. Anal. Chem. 1, 329–355.
Agilent, 2003. Agilent 4294A Precision Impedance Analyzer Operation Manual, 7th ed. Agilent Technologies.
Fosdick, L.E., Anderson, J.L., 1986. Anal. Chem. 58, 2481–2485.
Franks, W., Schenker, I., Schmutz, P., Hierlemann, A., 2005. IEEE Trans. Biomed. Eng. 52, 1295–1302.
Gómez, R., et al., 2006. Biomed. Microdevices 8 (1), 43–49.
Huang, X., Greve, D.W., Nguyen, D.D., Domach, M.M., 2003. Proc. IEEE Sens. 1, 304–309.
Ivorra, A., et al., 2003. Biosens. Bioelectron. 19 (4), 391–399.
Judy, J.W., 2001. Smart Mater. Struct. 10, 1115–1134.
Justin, G., Finley, S., Abdur Rahman, A., Guiseppi-Elie, A. Biomedical Microdevices, 2008 (online).
Lempka, S.F., Johnson, M.D., Barnett, D.W., Moffitt, M.A., Otto, K.J., Kipke, D.R., McIntyre, C.C., 2006. Engineering in Medicine and Biology Society 28th Annual International Conference of the IEEE.
Matysik, F.-M., Meister, A., Werner, G., 1995. Anal. Chim. Acta 305, 114–120.
McCoy, M.H., Wang, E., 2005. J. Virol. Methods 130, 157–161.
Min, J., Baeumner, Antje, J., 2004. Electroanalysis 16, 724–729.
Park, T.H., Shuler, M.L., 2003. Biotechnol. Prog. 19, 243–253.
Pejcic, B., De Marco, R., 2006. Electrochim. Acta 51, 6217–6229.
Rahman, A.R.A., Lo, C.M., Bhannsali, S., in press. IEEE Trans. Biomed. Eng.
Rahman, A.R.A., Price, D.T., Bhansali, S., 2007. Sens. Actuators B 127, 89–96.
Sagues, A.A., Kranc, S.C., 1996. American Society for Testing Materials, STP1276, pp. 58–73.
Sandison, M.E., Anicet, N., Glidle, A., Cooper, J.M., 2002. Anal. Chem. 74, 5717–5725.
Schwan, H.P., 1963. Biophysik 1, 198–208.
Wang, L., Wang, H., Wang, L., Mitchelson, K., Yu, Z., Cheng, J., 2008. Biosens. Bioelectron. 24, 14–21.
Yun, Y., et al., 2007. Nanotechnology 18, 465505, 7 pp.